

Layer-by-layer construction of graphene-based microbial fuel cell for improved power generation and methyl orange removal

Wei Guo · Yanrui Cui · Hong Song · Jianhui Sun

Received: 24 January 2014 / Accepted: 30 January 2014 / Published online: 19 February 2014
© Springer-Verlag Berlin Heidelberg 2014

Abstract Development of highly efficient anode is critical for enhancing the power output of microbial fuel cells (MFCs). The aim of this work is to investigate whether modification of carbon paper (CP) anode with graphene (GR) via layer-by-layer assembly technique is an effective approach to promote the electricity generation and methyl orange removal in MFCs. Using cyclic voltammetry and electrochemical impedance spectroscopy, the GR/CP electrode exhibited better electrochemical behavior. Scanning electron microscopy results revealed that the surface roughness of GR/CP increased, which was favorable for more bacteria to attach to the anode surface. The MFCs equipped with GR/CP anode achieved a stable maximum power density of 368 mW m^{-2} under $1,000 \Omega$ external resistance and a start time for the initial maximum voltage of 180 h, which were, respectively, 51 % higher and 31 % shorter than the corresponding values of the MFCs with blank anode. The anode and cathode polarization curves revealed negligible difference in cathode potentials but obviously difference in anode potentials, indicating that the GR-modified anode other than the cathode was responsible

for the performance improvement of MFC. Meanwhile, compared with MFCs with blank anode, 11 % higher decolorization efficiency and 16 % higher the chemical oxygen demand removal rate were achieved in MFC with GR-modified anode during electricity generation. This study might provide an effective way to modify the anode for enhanced electricity generation and efficient removal of azo dye in MFCs.

Keywords Microbial fuel cell · Anode modification · Graphene · Layer-by-layer assembly · Methyl orange · Decolorization

Introduction

Microbial fuel cells (MFCs) convert chemical energy to electrical energy via the catalysis of electroactive microorganisms. Recently, MFCs have gained an increasing attention due to their potential usage for simultaneous wastewater treatment and biomass-based energy production [1]. However, the relatively low power output was considered as one of the main obstacles for its further application. Amongst many factors affecting the performance of MFCs, the anode, which had great influence on the growth and activities of microbes as well as on the electron transfer rates, was considered as one of the key limiting factors [2, 3]. Therefore, developing effective anode materials remains critical for enhancing the current output of MFCs.

To date, researchers have employed various commercially available graphite-based materials such as carbon cloth or carbon paper (CP) as anode materials due to their good biocompatibility, conductivity, stability, and low cost [4]. However, these materials possess limited surface areas

W. Guo · Y. Cui · H. Song · J. Sun (✉)
School of Environment, Henan Normal University, Key
Laboratory for Yellow River and Huai River Water
Environmental and Pollution Control Ministry of Education,
Henan Normal University, Xinxiang 453007, People's Republic
of China
e-mail: sunjh@htu.cn

W. Guo · Y. Cui · H. Song · J. Sun
Henan Key Laboratory for Environmental Pollution Control,
Xinxiang 453007, People's Republic of China

W. Guo
Department of Chemistry, Xinxiang Medical University,
Xinxiang 453003, People's Republic of China

and relatively small electrochemical activities, retarding the interaction between microorganisms and the anode surface [5, 6]. To tackle this concern, anode modification by introducing functional groups onto the anode surface [7], or by combining with certain electroactive materials, such as conducting polymers [8, 9], carbon nanotubes (CNTs) [10, 11], metal nanoparticles [12, 13], and metal oxide nanoparticles [14, 15], has been attempted in this regard, which was proven to be effective to enhance the power generation of MFCs.

Graphene (GR), a flat monolayer of carbon atoms tightly packed into a two-dimensional honeycomb lattice, has been widely used in various applications in modified electrodes, electrocatalysis, and electrochemical sensors because of its unique electrochemical properties and electrocatalytic activities [16, 17]. Recently, research in the field of MFCs had proved graphene to be a promising electrocatalyst material. For example, Liu et al. [18] designed the GR-modified carbon cloth anode and showed that the graphene modification improved the power density and energy conversion efficiency by 2.7 and 3 times, respectively. A recent study performed by Zhao et al. [19] on using the ionic liquid functionalized GR-modified anode in MFCs revealed that the MFC with the modified anode produced a maximum power density of 601 mW m^{-2} , which was 4.2 times higher than that of the MFCs equipped with unmodified carbon paper (142 mW m^{-2}).

A number of approaches had been explored to assemble GR on the anodes in MFCs with tailorable properties and architectures, including chemical vapor deposition of GR using a nickel foam as the substrate [20], direct deposition of GR by casting its suspension on the surface of the electrode [21, 22], electrochemical reduction of graphene oxide (GO) to GR from a suspension containing GO or from a GO film on the electrode surface [18, 23]. To the best of our knowledge, no study on the preparation of GR-modified anode by an electrostatic layer-by-layer assembly method and on its corresponding MFC performances has been reported by far. The layer-by-layer technique relies mainly on the alternating adsorption of oppositely charged species, offering a facile and effective way to build up uniformly nanostructured films with controllable morphologies and thickness.

On the other hand, azo dyes, encompassing the largest group of synthetic dyes extensively used in textile dyeing and paper printing, have been deemed as refractory pollutants constituting a significant burden on the environment [24]. Recent years, MFCs have exhibited their ability to remove azo dyes and to simultaneously generate electrical power [25, 26]. Herein, we demonstrate a simple strategy for constructing the GR-modified carbon paper electrodes via a layer-by-layer assembly method through the electrostatic adsorption between positively charged

polyethyleneimine (PEI) and negatively charged GR. The electrochemical performances of the electrodes have been studied with the aid of cyclic voltammetry (CV) and electrochemical impedance spectroscopy (EIS), and improved electron transfer ability of the modified electrode has been observed compared to that of the blank carbon paper anode. Morphology study has revealed that our GR-modified anode possessed large surface areas, beneficial to the attachment of bacteria. Consequently, the usage of our GR-modified anode has enabled the improvement of the biocurrent generation and methyl orange (MO) decolorization in MFCs.

Materials and methods

Chemicals

Carbon paper was purchased from Shanghai Hesen Engineering Co. Ltd. Cation exchange membranes (CMI-7000) were obtained from Ankatech Membrane Separation Engineering & Technology Co. Ltd. Polyethyleneimine (PEI) (M.W. 60,000, 50 wt% aq. solution, branched) was purchased from J&K Chemical Ltd., China. Methyl orange ($\text{C}_{14}\text{H}_{14}\text{N}_3\text{SO}_3\text{Na}$) was purchased from Beijing Chemical Reagent Co. (Beijing, China). All chemicals were of analytical reagent grade and used without further purification. Deionized water was used throughout the study.

Electrode preparation

The GR used in this study was synthesized and characterized according to our reported recipe [27], which mainly involved the conversion of graphene oxide (GO) to GR. The as-prepared GR was fully dispersed in water by ultrasonication (480 W, 40 kHz) for 2 h to form dispersed solution with a concentration of 0.5 mg mL^{-1} .

Prior to fabricating GR/CP anode, carbon papers were first soaked in acetone for a period of 4 h to remove adsorbed organic contaminations and then soaked in 1 mol L^{-1} HCl and 1 mol L^{-1} NaOH solution for 24 h to wipe out possible impurities. After that, the carbon paper electrode was pretreated with concentrated $\text{H}_2\text{SO}_4\text{--HNO}_3$ (volume ratio: 3:1) for 1 h to introduce carboxyl groups on the surface, giving rise to the formation of a hydrophilic and negatively charged surface [28]. The functionalized carbon paper electrode was then alternately immersed for 20 min in the positively charged PEI aqueous solution (10 mg mL^{-1}) and the negatively charged GR suspension, followed by water washing and hot air drying, resulting in a PEI/GR layered structure. This cycle was repeated to obtain the desired number of bilayers (n) for $\{\text{PEI/GR}\}_n$ layer-by-layer films, and the multilayer film-modified

electrode was ready for electrochemical and morphological analysis. To highlight the role played by the GR in the performance of MFCs, blank carbon paper electrodes were used to serve as a reference blank. The blank carbon paper electrodes were prepared by the same procedure as described above, but without PEI/GR layer-by-layer assembly. For MFCs studies, {PEI/GR}₆ film-modified anode was used.

Characterization

A CHI 660d electrochemical workstation (CH Instruments) was used for CV and EIS analysis. A regular three-electrode cell was used with a saturated calomel electrode (SCE) as the reference electrode, a platinum wire as the counter electrode, and a modified carbon paper electrode or a blank carbon paper electrode as the working electrode. EIS measurements were performed in the frequency range from 100 kHz to 1 Hz with sinusoidal perturbation of 5 mV amplitude under the formal potential of $\text{Fe}(\text{CN})_6^{3-/4-}$ (0.18 V vs. SCE), and the obtained data were analyzed using ZSimpWin 3.10 software.

The assembled electrodes with different PEI/GR bilayers were characterized with the aid of a UV–Vis spectrometer (Beijing Purkinje General Instrument Co., Ltd, China). For UV–Vis spectroscopic measurements, quartz slides ($1.2 \times 4.5 \text{ cm}^2$, 1 mm thick) were pretreated with piranha solution (3:7 volume ratio of 30 % H_2O_2 and concentrated H_2SO_4) for about 30 min and then rinsed with water. The following procedure for fabricating layer-by-layer films was the same as that on carbon paper surface, and after completion of each assembly cycle on a quartz slide UV–Vis spectroscopy was carried out using an air blank for all the measurements.

The surface morphology of the samples was inspected using a JSM-6390LV scanning electron microscopy (SEM) (JEOL Ltd., Japan) and a KYKY-EM3200 scanning electron microscopy (KYKY technology Co. Ltd., China). Zeta potential analysis was performed using a nano-ZS90 zeta-sizer (Malvern Instruments Ltd., UK).

Construction and operation of MFCs

The two-chambered MFC was made of perspex material (Fig. 1) and consisted of an anode chamber and a cathode chamber, each with an operating volume of 140 mL ($7 \text{ cm} \times 5 \text{ cm} \times 4 \text{ cm}$). The anodes were constructed with either blank carbon papers or GR-modified carbon papers ($5 \times 3 \text{ cm}^2$) and all the cathodes were just carbon papers ($5 \times 3 \text{ cm}^2$). CMI-7000 cation exchange membrane was sandwiched between the two chambers and held together by an external metal screw. Rubber gaskets were used to secure the sealing between the perspex material and the

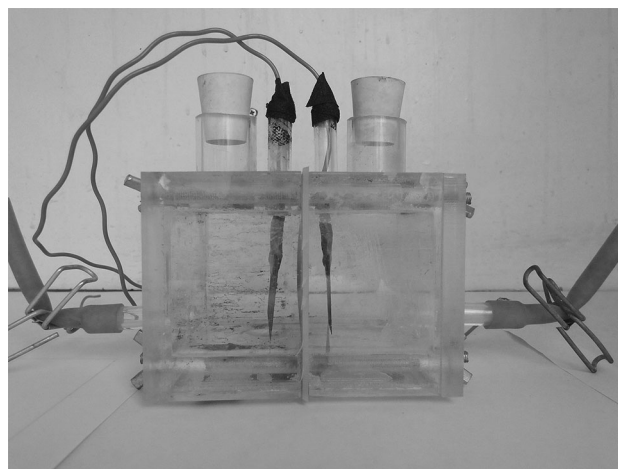


Fig. 1 Photograph of the two-chambered MFC

membrane. Copper wires were used to connect the circuit with an external resistance of $1,000 \ \Omega$. $100 \text{ mmol L}^{-1} \text{K}_3[\text{Fe}(\text{CN})_6]$ in 50 mmol L^{-1} phosphate buffer solution (PBS, pH 7.0) was used as the electron acceptors [29, 30].

Anaerobic sludge was inoculated as the anodic inoculums of MFCs, which was collected from a local wastewater treatment plant (Xinxiang, Henan, China). A cultivation solution added to the anode chamber for bacterial growth contained 1 g L^{-1} glucose as electron donors; 50 mmol L^{-1} PBS (pH 7.0) containing (per liter deionized water): 3.32 g $\text{NaH}_2\text{PO}_4 \cdot 2\text{H}_2\text{O}$, 10.32 g $\text{Na}_2\text{HPO}_4 \cdot 12\text{H}_2\text{O}$, 0.13 g KCl, 0.31 g NH_4Cl , 12.5 mL vitamins and 12.5 mL mineral solution. The initial pH of anolyte was 6.8–7.0. The inoculated anaerobic sludge was set to account for 25 % (volume ratio) of the whole anode solution. All MFCs were operated in batch cycle mode. The anode solution was replaced by fresh cultivation solution when the voltage decreased below 50 mV and N_2 gas was flushed continuously for 15 min to remove dissolved oxygen in the anodic chamber before each batch test. All MFC experiments were conducted at $30 \pm 1 \text{ }^\circ\text{C}$ in a constant temperature room. Since the biological fluctuation of the anaerobic sludge and other MFC experimental conditions could affect the outcomes. Three parallel groups of experiments were carried out, where their average values of the results were taken.

Analytics and calculations

Voltage and polarization curve

The voltage of the MFCs was measured every 30 min with a digital multimeter, and all the data were automatically recorded by a computer. Polarization curves were obtained by changing external circuit resistance from 10,000 to $50 \ \Omega$.

The current density, I_A ($A\ m^{-2}$) and the power density, P_A ($W\ m^{-2}$) of the system can be calculated using the formula:

$$I_A = \frac{V}{R \cdot A} \quad (1)$$

$$P_A = \frac{V^2}{R \cdot A} \quad (2)$$

where V (V) is the cell voltage, R (Ω) is the external resistances and A (m^2) is the projected area of the anode.

Removal of methyl orange

The removal of methyl orange (MO) was monitored by withdrawing samples at a time interval of 2 h during one cycle and immediately centrifuged (4,000 rpm) for 15 min to remove suspended biomass from the anode solution. If needed, sample solution was diluted before each measurement. The blank solution was the anode solution taken from the MFC without the addition of MO, and the following procedures for pretreatment were the same as the samples. The decolorization efficiency of MO was tested in terms of the changes of the UV–Vis absorbance at $\lambda_{max} = 465\ nm$ using a UV–Vis spectrophotometer with a 1-cm path length spectrometric quartz cell. Decolorization efficiency can be calculated by:

$$\text{decolorization efficiency}(\%) = \frac{A_0 - A_t}{A_0} \times 100\% \quad (3)$$

where A_0 is the absorbance of the initial solution taken from the anode chamber, and A_t is the absorbance of solution taken from the anode chamber at a certain reaction time t (min).

The chemical oxygen demand (COD) removal rate of the dye solution was measured by the decrease of COD of the dye solution, which can be estimated by the following expression. COD was measured according to the standard dichromate titration method [31].

$$\text{COD removal rate}(\%) = \frac{COD_0 - COD_t}{COD_0} \times 100\% \quad (4)$$

where COD_0 is the COD of the initial solution taken from the anode chamber, and COD_t is the COD of the solution taken from the anode chamber at a certain reaction time t (min).

Results and discussion

Zeta potential of the synthesized GO and GR

Zeta potential of the prepared GO and GR were measured to be -40.8 and -25.4 mV, respectively. After GO

reduction, a significantly positive shift of 15.4 mV was observed, indicating that GO was successfully reduced by chemical reagent, where the amounts of the negatively charged groups (such as hydroxyl, carboxyl and epoxy groups) on the edges and surface of GO decreased. On the other hand, a small quantity of these negatively charged groups still remained on its surface, facilitating the assembly of the as-prepared, negatively charged GR with PEI to build multifunctional nanostructures by a layer-by-layer technique [32].

Characterization of GR/CP electrode

UV–Vis spectroscopy

On the basis of electrostatic interactions, $\{PEI/GR\}_n$ films were prepared by alternatively depositing PEI and GR from their dipping solution or suspension. The process of layer-by-layer assembly on quartz slides had been monitored by UV–Vis spectroscopy, as shown in Fig. 2. It can be seen that the spectra of $\{PEI/GR\}_n$ films display an absorption peak at 280 nm, which is regarded as the trademark for chemically reduced GR [33]. The intensities of the characteristic band increase gradually with the growing number of bilayers, revealing the successful deposition of $\{PEI/GR\}_n$ films. The linear relationship ($r = 0.9997$) between the absorbance at 280 nm with the number of bilayers (inset of Fig. 2) further suggests that almost identical amount of GR was loaded in each assembling step, leading to the construction of uniform multilayer film.

Cyclic voltammetry

CV measurements of the multilayer film electrode were performed during the assembly process. Figure 3 shows the

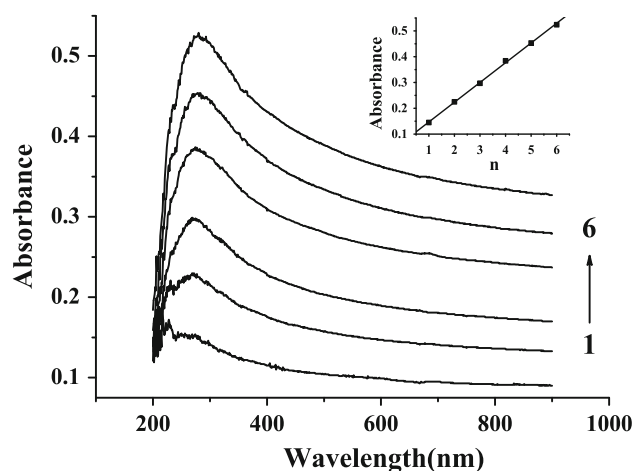


Fig. 2 UV–Vis spectra of $\{PEI/GR\}_n$ films assembled on quartz slides with different number of bilayers (n , $n = 1$ –6). Inset is the dependence of absorbance of GR at 280 nm on the number of bilayers

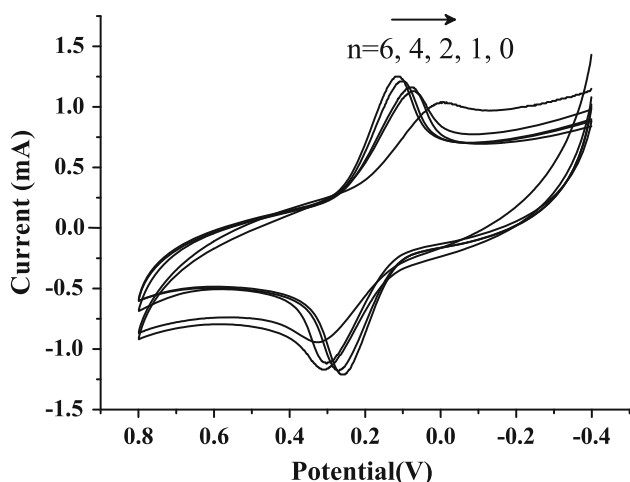


Fig. 3 Cyclic voltammograms of $\{\text{PEI/GR}\}_n$ ($n = 0, 1, 2, 4, 6$) multilayer-modified carbon paper electrode in aqueous 0.1 mol L^{-1} KCl containing 10 mmol L^{-1} $\text{K}_3[\text{Fe}(\text{CN})_6]$ at a scan rate of 20 mV s^{-1} . $n = 0$ referred to blank carbon paper electrode

cyclic voltammograms of blank carbon paper electrode and GR-modified carbon paper electrode with bilayer number (n) from 1 to 6 in a 0.1 mol L^{-1} KCl solution containing 10 mmol L^{-1} $\text{K}_3[\text{Fe}(\text{CN})_6]$ (used as the redox electrochemical probe). A pair of well-defined, nearly reversible reduction–oxidation peaks can be observed at 0.18 V on both types of electrodes, which correspond to the $\text{Fe}(\text{CN})_6^{3-}/\text{Fe}(\text{CN})_6^{4-}$ redox couple. Meanwhile, apparent differences between the two pair of peaks can also be identified. First, both the anodic and cathodic peak currents for GR-modified electrode enhance remarkably in comparison with those of the blank carbon paper electrode; moreover, the redox peak height of GR-modified electrode increases with the growing layer number, which is in good agreement with the results from the UV–Vis measurements. Second, since the peak-to-peak separation (ΔE_p) between the anodic and cathodic peaks is inversely proportional to the rate of electron transfer, a smaller ΔE_p represents an increase in the electron transfer rates [34]. As shown in Fig. 3, the value of ΔE_p of the GR-modified carbon paper electrode is smaller than that of the blank carbon paper electrode, indicating an enhancement of the electron transfer rate and hence a superior electrochemical behavior occurred in the GR-modified carbon paper electrode, probably owing to the incorporation of GR, which offers an advanced conductivity as well as an increased electroactive surface area [35].

Electrochemical impedance spectroscopy

EIS, a powerful tool to probe the features of surface-modified electrode, was employed to monitor the modifying process of electrodes and study the effect of the

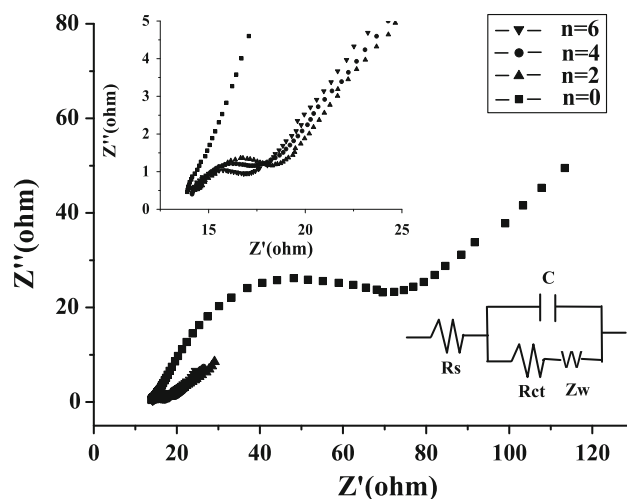


Fig. 4 Nyquist plots and equivalent circuit of $\{\text{PEI/GR}\}_n$ multilayer films assembled on carbon paper electrode in 0.1 mol L^{-1} KCl containing 10 mmol L^{-1} $\text{K}_3[\text{Fe}(\text{CN})_6]$, $n = 0$ (filled square), 2 (filled triangle), 4 (filled circle), 6 (filled inverted triangle). $n = 0$ referred to blank carbon paper electrode. The inset illustrates the high-frequency part of the result

introduction of GR on the electrode interfacial resistance. Figure 4 shows the impedance spectra in the form of Nyquist diagrams for blank or GR-modified carbon paper electrodes in 0.1 mol L^{-1} KCl containing 10 mmol L^{-1} $\text{K}_3[\text{Fe}(\text{CN})_6]$ (used as the redox electrochemical probe), where the inset depicts the high-frequency part of the result. It is known that the electron transfer resistance (R_{ct}) of the electrochemical reaction at electrode/electrolyte interface, which corresponds to the semicircle diameter of the Nyquist plot, reveals the electron transfer kinetics of the redox electrochemical probe at the electrode interface [34]. The values of R_{ct} can be estimated using the Randles equivalent circuit as the model and fitting the impedance data into the model. The R_{ct} value for the blank carbon paper electrode was calculated to be 42.14Ω . After GR modification, prominent decreases of the value of the R_{ct} occurred to reach 16.71 , 15.82 , and 14.52Ω for 2, 4, and 6 layers, respectively. Since a smaller value of R_{ct} indicates a faster electron transfer rate between electrode and electrolyte [34], the apparent reduction in R_{ct} values for the GR-modified carbon paper electrode therefore implies that the incorporation of GR into the multilayer film significantly reduces the electron transfer resistance and realizes a faster electrochemical reaction between the electrode and electrolyte. Moreover, it can be seen from the inset of Fig. 4 that the straight line region over low frequency of the GR-modified carbon paper electrode is significantly smaller than that of blank carbon paper electrode. The straight line region is characteristic of a diffusion-limiting step in an electrochemical process [34]. The results herein indicate that GR-modified carbon paper electrodes provide

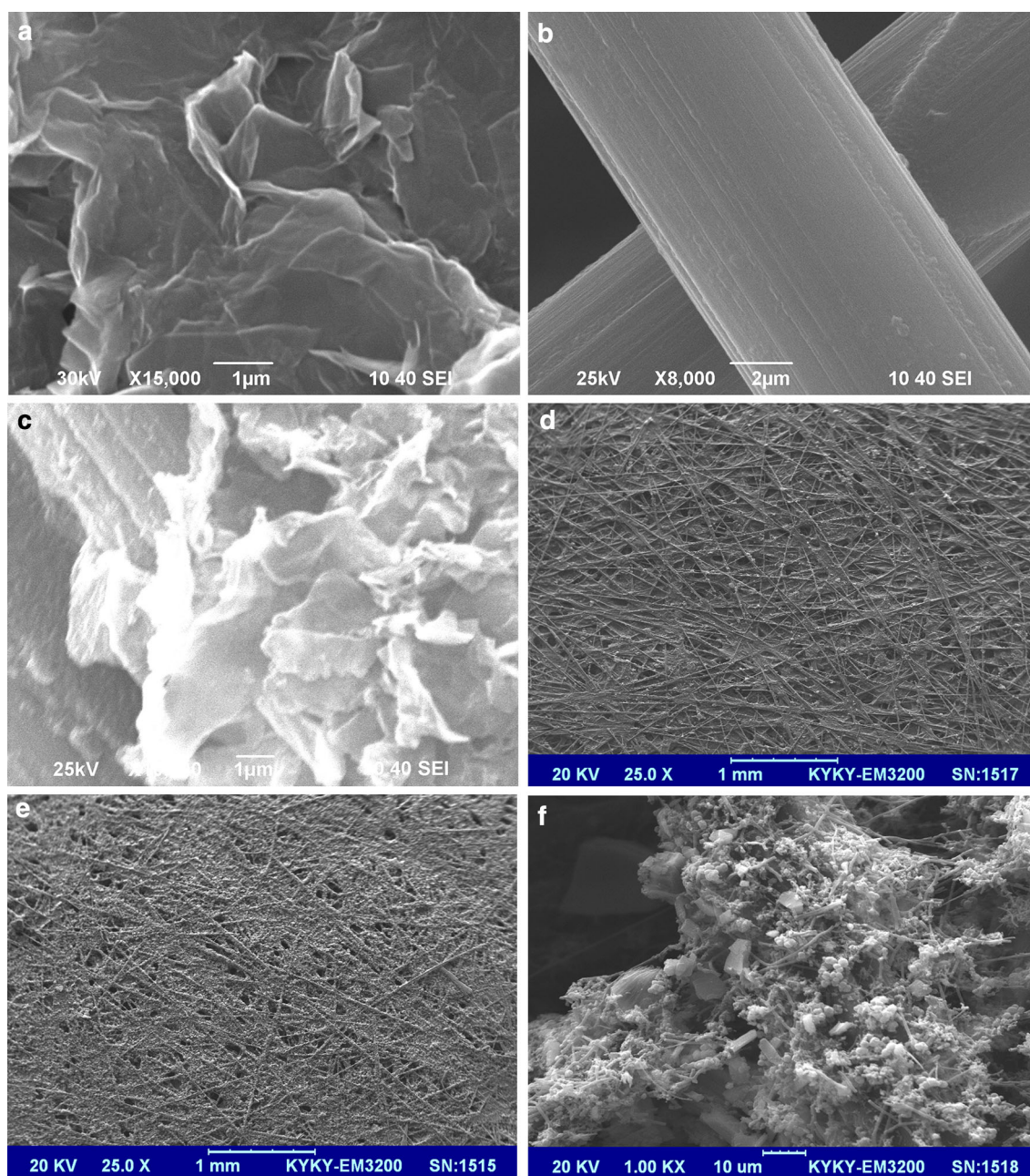


Fig. 5 SEM images of GR (a), the blank carbon paper (b), the GR-modified carbon paper (c) and the biofilm on the blank carbon paper (d) and on the GR-modified carbon paper at low (e) and high (f) magnifications

a proper accommodation for reactants to access the reaction centers [36], therefore improving the diffusion of electrolyte toward the surface of the electrode.

Scanning electron microscopy

The surface morphologies of the GR/CP electrodes used in this work were characterized by SEM. The SEM micrograph in Fig. 5a shows the obtained GR materials, where the flake-like GR sheets can be observed. Figure 5b is the

SEM image of the blank carbon paper, which consists of a number of carbon fibers with relatively smooth surfaces. Figure 5c shows the morphology of the GR-modified carbon paper, clearly revealing the typically wrinkled GR sheet structure with slightly scrolled edges, which is beneficial to the enlargement of the electrode areas. SEM images of bacteria-attached carbon paper anodes are depicted in Fig. 5d–f. It can be observed that there are more bacteria attached to the GR-modified carbon paper anode (Fig. 5e, f) compared to that of the blank carbon

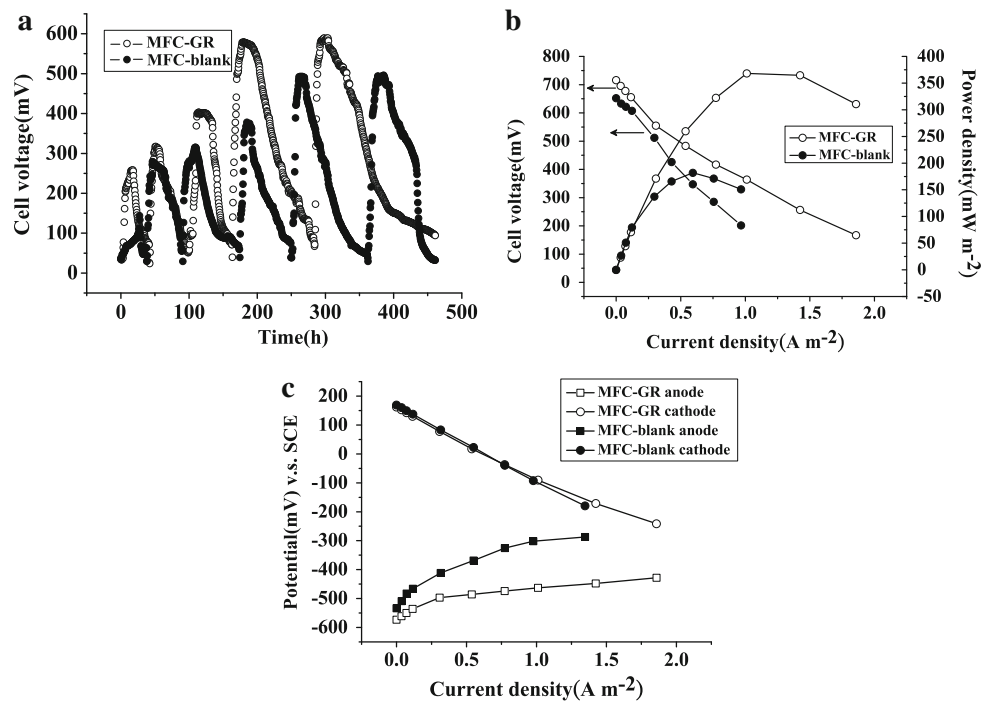


Fig. 6 Performance of MFCs with a GR-modified carbon paper anode and a blank carbon paper anode under 1,000 Ω resistance: **a** cell voltage output as a function of time, **b** power density and cell polarization curves, and **c** anode and cathode polarization curves

paper anode (Fig. 5d), indicating that GR is helpful to induce the adsorption and growth of specific microbial on the electrode surface.

Performances of MFCs

Electricity generation

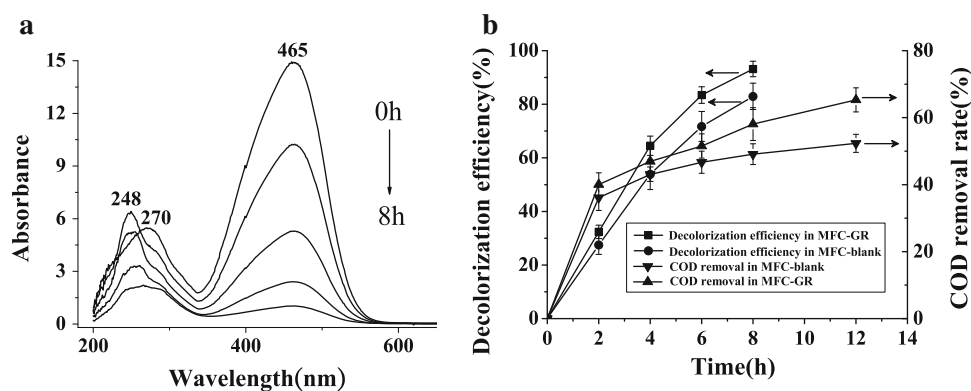
The performances of both blank CP and GR/CP anode-based MFCs were evaluated by measuring the output voltage at a constant external circuit resistance (1,000 Ω). MFCs equipped with GR/CP anodes (MFC-GR) achieved much better performance than that prepared with blank CP anode (MFC-blank). Figure 6a shows a representative cycle. After inoculation, stable maximum voltages of 490 and 580 mV are obtained for the MFC-blank and MFC-GR, respectively. Within a lag time of about 50 h during the first cycles, the MFC-GR reaches a maximum voltage of 250 mV, which is 1.7 times as high as that of MFC-blank (150 mV). Moreover, the start time for the initial maximum stable voltage is 180 h for the MFC-GR compared to that at 260 h for MFC-blank, shortened by 31 % and the MFC-GR delivers a maximum stable voltage of 580 mV, which is 15 % greater than that of MFC-blank (490 mV). Based on the CV, EIS, and SEM studies, it can be speculated that the GR-modified anode possesses the larger specific surface area for the biofilm growth and facilitates the electron transfer from the electrolyte to the electrode as well as

inside the electrode, leading to a better performance of the MFC-GR in terms of electricity generation.

Figure 6b shows the polarization curves and power density curves of both types of MFCs. Although both types of MFCs exhibit quite similar behaviors in the open circuit voltage, the maximum power density of the MFC-GR apparently improves compared with that of the MFC-blank. With the external resistance varied from 10,000 to 50 Ω, the MFC-blank achieves a maximum power density of 182 mW m⁻² at the current density of 0.59 A m⁻², whilst the maximum power density of the MFC-GR reaches 368 mW m⁻² at the current density of 1.01 A m⁻², twice larger than that generated by the MFC-blank. The polarization curves further verify that GR modification strategy indeed affects the performances of MFCs and improves the power output.

Figure 6c displays the comparison between the anode and cathode polarization curves of the MFC-GR and the MFC-blank. It can be seen that the two MFCs exhibit almost the same features in their cathode potentials due to the identical cathode used in both types of MFCs. However, the anode open circuit potential (OCPa) and anode polarization curves differ from each other, suggesting that the anode potential is greatly affected by the modification of GR. The OCPa (versus SCE) moves toward more negative values from -534 mV (MFC-blank) to -573 mV (MFC-GR), and a decreased slope of the anode polarization curve can be found in MFCs using the GR-

Fig. 7 **a** UV–Vis spectra of MO during the decolorization process in MFC–GR; **b** Decolorization efficiency and COD removal rate of 300 mg L⁻¹ MO in MFCs equipped with GR-modified anode (filled square and filled triangle) and blank anode (filled circle and filled inverted triangle). Time zero meant the beginning of the cycles in which the MO removal tests were conducted



modified anode compared to those using the blank anode. With the increase of the current density from 0 to 1.35 A m⁻², the anode potential of MFC-blank decreases by 46 % from -534 to -287 mV, indicating that a larger overpotential would be required for the bioelectrochemical reaction at high currents [37], whilst the anode potential of the MFC-GR only decreases by 25 % from -573 to -428 mV. The lower anode overpotential with the GR-modified anode reflects the positive role played by GR in enhancing the bioelectroactivity of the anode [38]. These results also reveal that the differences in the performances of the two types of MFCs originate from the distinct types of materials employed in the anode and do not from the cathode.

Methyl Orange (MO) removal in MFCs

Removal performances of MO (300 mg L⁻¹) in MFCs equipped with GR-modified anode and blank anode are shown in Fig. 7. It can be observed from Fig. 7a that the typical UV–Vis spectra of MO during decolorization in MFC–GR and MFC-blank show the similar trends. The absorption spectrum of the original anode solution is characterized by the main band in the visible region with its maximum absorption at 465 nm and by the band in the ultraviolet region located at 270 nm. The absorbance peak at 465 nm is attributed to the azo bonds of MO molecule, whilst the absorbance peak at 270 nm is ascribed to the $\pi \rightarrow \pi^*$ transition related to aromatic rings [39]. After 2 h reaction, the intensities of the bands at both 465 and 270 nm become weaker, but a new band at 248 nm associated with sulfanilic acid [24] appears. The change of the spectra reveals the cleavage of the azo bond and the formation of the reaction intermediates during the decolorization of MO in MFCs.

Although MO could be removed in both reactors, MFC-GR achieves better removal performance than that of MFC-blank at any sampling interval during the course of reaction. According to the changes of absorbance at

465 nm, it can be seen from Fig. 7b that the decolorization efficiency of MO solutions (300 mg L⁻¹) in MFC–GR and MFC-blank after 4 h reaction reaches 53 and 64 %, respectively. Meanwhile, COD removal rate increases with the increase of reaction time, almost 68 % COD removal rate is achieved within 10 h reaction time for MFC–GR, whilst 52 % for MFC-blank. The better performance of MO removal in MFC–GR might be caused by the different capacities of electricity generation of MFCs with the employment of different anodes. At the anode of a MFC, organic cosubstrate (like glucose, acetate or sucrose, glucose in this work) is oxidized by electrochemically active microorganisms, followed by the transfer of generated electrons to the anode which then pass through an external circuit to the cathode, thus producing current. When azo dye is added into the anode chamber, the reductive cleavage of azo bond in the structure of azo dye would consume partly the electrons from cosubstrate oxidation [40]. On a basis of the principles of electricity generation in MFC, the decolorization mechanism of MO, and the results of the output voltage in these two types of reactors, it is not difficult to deduce that more electrons are discharged from cosubstrate oxidation in the anode chamber of MFC–GR, and consequently, more electrons would be consumed by azo dye, resulting in a better decolorization performance.

Conclusions

In summary, we have employed a facile layer-by-layer assembly method to modify the anode of MFCs with GR and achieved an enhanced MFC performance with regard to the electricity generation and MO removal. Through our investigation we have speculated that the advanced performance of MFCs is associated with the unique properties of GR such as large specific surface area and excellent conductivity upon its incorporation, which is beneficial to the attachment of bacteria to the electrode and the improvement of the electron

transfer rate. Our study might offer special insights into designing facile and effective route for the construction of MFCs for achieving promising electricity generation as well as efficient treatment of azo dye wastewater.

Acknowledgments The authors are grateful to the financial support from the Plan for Scientific Innovation Talent of Henan Province (Grant No. 134200510014), the Basic and Cutting-Edge Technology Research Project of Henan province (Grant No. 112300410157), and the Innovation Scientists and Technicians Troop Construction Projects of Henan Province.

References

- Logan BE, Aelterman P, Hamelers B, Rozendal R, Schröder U, Keller J, Freguac S, Verstraete W, Rabaey K (2006) Microbial fuel cells: methodology and technology. *Environ Sci Technol* 40:5181–5192
- Cheng SA, Liu H, Logan BE (2006) Increased power generation in a continuous flow MFC with advective flow through the porous anode and reduced electrode spacing. *Environ Sci Technol* 40:2426–2432
- Katuri K, Ferrer ML, Gutierrez MC, Jimenez R, del Monte F, Leech D (2011) Three-dimensional microchanneled electrodes in flow-through configuration for bioanode formation and current generation. *Energy Environ Sci* 4:4201–4210
- Wang X, Cheng SA, Feng YJ, Merrill MD, Saito T, Logan BE (2009) Use of carbon mesh anodes and the effect of different pretreatment methods on power production in microbial fuel cells. *Environ Sci Technol* 43:6870–6874
- Cai H, Wang J, Bu YF, Zhong Q (2013) Treatment of carbon cloth anodes for improving power generation in a dual-chamber microbial fuel cell. *J Chem Technol Biotechnol* 88:623–628
- Ci SQ, Wen ZH, Chen JH, He Z (2012) Decorating anode with bamboo-like nitrogen-doped carbon nanotubes for microbial fuel cells. *Electrochem Commun* 14:71–74
- Luo JM, Chi ML, Wang HY, He HH, Zhou MH (2013) Electrochemical surface modification of carbon mesh anode to improve the performance of air-cathode microbial fuel cells. *Bioprocess Biosyst Eng* 36:1889–1896
- Lai B, Tang XH, Li HR, Dua ZW, Liu XW, Zhang Q (2011) Power production enhancement with a polyaniline modified anode in microbial fuel cells. *Biosens Bioelectron* 28:373–377
- Wang YQ, Li B, Zeng LZ, Cui D, Xiang XD, Li WS (2013) Polyaniline/mesoporous tungsten trioxide composite as anode electrocatalyst for high-performance microbial fuel cells. *Biosens Bioelectron* 41:582–588
- Sun JJ, Zhao HZ, Yang QZ, Song J, Xue A (2010) A novel layer-by-layer self-assembled carbon nanotube-based anode: preparation, characterization, and application in microbial fuel cell. *Electrochim Acta* 55:3041–3047
- Xie X, Hu LB, Pasta M, Wells GF, Kong DS, Criddle CS, Cui Y (2011) Three-dimensional carbon nanotube-textile anode for high-performance microbial fuel cells. *Nano Lett* 11:291–296
- Sun M, Zhang F, Tong ZH, Sheng GP, Chen YZ, Zhao Y (2010) A gold-sputtered carbon paper as an anode for improved electricity generation from a microbial fuel cell inoculated with *Shewanella oneidensis* MR-1. *Biosens Bioelectron* 26:338–343
- Xu ST, Liu H, Fan YZ, Schaller R, Jiao J, Chaplen F (2012) Enhanced performance and mechanism study of microbial electrolysis cells using Fe nanoparticle-decorated anodes. *Appl Microbiol Biot* 93:871–880
- Peng XH, Yu HB, Wang X, Zhou QX, Zhang SJ, Geng LJ (2012) Enhanced performance and capacitance behavior of anode by rolling Fe₃O₄ into activated carbon in microbial fuel cells. *Bioresour Technol* 121:450–453
- Ozkaya B, Akoglu B, Karadag D, Acı G, Taskan E, Hasar H (2012) Bioelectricity production using a new electrode in a microbial fuel cell. *Bioprocess Biosyst Eng* 35:1219–1227
- Chen D, Tang LH, Li JH (2010) Graphene-based materials in electrochemistry. *Chem Soc Rev* 39:3157–3180
- Gan T, Hu SS (2011) Electrochemical sensors based on graphene materials. *Microchim Acta* 175:1–19
- Liu J, Qiao Y, Guo CX, Lim S, Song H, Li CM (2012) Graphene/carbon cloth anode for high-performance mediatorless microbial fuel cells. *Bioresour Technol* 114:275–280
- Zhao C, Wang Y, Shi FJ, Zhang JR, Zhu JJ (2013) High bio-current generation in *Shewanella*-inoculated microbial fuel cells using ionic liquid functionalized graphene nanosheets as an anode. *Chem Commun* 49:6668–6670
- Yong YC, Dong XC, Chan-Park MB, Song H, Chen P (2012) Macroporous and monolithic anode based on polyaniline hybridized three-dimensional graphene for high-performance microbial fuel cells. *ACS Nano* 6:2394–2400
- Xiao L, Damiana J, Luo JY, Jang HD, Huang JX, He Z (2012) Crumpled graphene particles for microbial fuel cell electrodes. *J Power Sources* 208:187–192
- Zhang YZ, Mo GQ, Li XW, Zhang WD, Zhang JQ, Ye JS, Huang XD, Yu CZ (2011) A graphene modified anode to improve the performance of microbial fuel cells. *J Power Sources* 196:5402–5407
- Hou JX, Liu ZL, Zhang PY (2013) A new method for fabrication of graphene/polyaniline nanocomplex modified microbial fuel cell anodes. *J Power Sources* 224:139–144
- Fan J, Guo YH, Wang JJ, Fan MH (2009) Rapid decolorization of azo dye methyl orange in aqueous solution by nanoscale zero-valent iron particles. *J Hazard Mater* 166:904–910
- Solanki K, Subramanian S, Basu S (2013) Microbial fuel cells for azo dye treatment with electricity generation: a review. *Bioresour Technol* 131:564–571
- Sun J, Li YM, Hu YY, Hou B, Zhang YP, Li SZ (2013) Understanding the degradation of Congo red and bacterial diversity in an air-cathode microbial fuel cell being evaluated for simultaneous azo dye removal from wastewater and bioelectricity generation. *Appl Microbiol Biotechnol* 97:3711–3719
- Dong SY, Sun JY, Li YK, Yu CF, Li YH, Sun JH (2014) ZnSnO₃ hollow nanospheres/reduced graphene oxide nanocomposites as high-performance photocatalysts for degradation of metronidazole. *Appl Catal B: Environ* 144:386–393
- Yu HH, Cao T, Zhou LD, Gu ED, Yu DS, Jiang DS (2006) Layer-by-layer assembly and humidity sensitive behavior of poly(ethyleneimine)/multiwall carbon nanotube composite films. *Sens Actuators B: Chem* 119:512–515
- Oh S, Min B, Logan BE (2004) Cathode performance as a factor in electricity generation in microbial fuel cells. *Environ Sci Technol* 38:4900–4904
- Wei LL, Han HL, Shen JQ (2012) Effects of cathodic electron acceptors and potassium ferricyanide concentrations on the performance of microbial fuel cell. *Int J Hydrogen Energy* 37:12980–12986
- Arnold G (2005) Standard methods for the examination of water and wastewater, 21st edn. American Public Health Association (APHA), Washington, DC
- Liu Y, Liu Y, Feng HB, Wu YM, Joshi L, Zeng XQ, Li JH (2012) Layer-by-layer assembly of chemical reduced graphene and carbon nanotubes for sensitive electrochemical immunoassay. *Biosens Bioelectron* 35:63–68

33. Sheng KX, Bai H, Sun YQ, Li C, Shi GQ (2011) Layer-by-layer assembly of graphene/polyaniline multilayer films and their application for electrochromic devices. *Polymer* 52:5567–5572
34. Bard AJ, Faulkner LR (2001) *Electrochemical methods: fundamentals and applications*, 2nd edn. Wiley, New York
35. Qiao Y, Bao SJ, Li CM, Cui XQ, Lu ZS, Guo J (2008) Nanostructured polyaniline/titanium dioxide composite anode for microbial fuel cells. *ACS Nano* 2:113–119
36. Qiao Y, Li CM, Bao SJ, Bao QL (2007) Carbon nanotube/polyaniline composite as anode material for microbial fuel cells. *J Power Sources* 170:79–84
37. Feng CH, Ma L, Li FB, Mai HJ, Lang XM, Fan SS (2010) A polypyrrole/anthraquinone-2,6-disulphonic disodium salt (PPy/AQDS)-modified anode to improve performance of microbial fuel cells. *Biosens Bioelectron* 25:1516–1520
38. Ci SQ, Wen ZH, Chen JH, He Z (2012) Decorating anode with bamboo-like nitrogen-doped carbon nanotubes for microbial fuel cells. *Electrochem Commun* 14:71–74
39. Galindo C, Jacques P, Kalt A (2000) Photodegradation of the aminoazobenzene acid orange 52 by three advanced oxidation processes: UV/H₂O₂, UV/TiO₂ and VIS/TiO₂: comparative mechanistic and kinetic investigations. *J Photochem Photobiol A: Chem* 130:35–47
40. Cao YQ, Hu YY, Sun J, Hou B (2010) Performance improvement of air-cathode single-chamber microbial fuel cell using a mesoporous carbon modified anode. *Bioelectrochem* 79:71–76